Res Chem Intermed
DOI 10.1007/s11164-015-2412-8

Synthesis of indole–quinoline–oxadiazoles: their anticancer potential and computational tubulin binding studies

Pooja R. Kamath[1] · Dhanya Sunil[1] · Abdul A. Ajees[2]

Received: 3 October 2015 / Accepted: 28 December 2015

Abstract Small hybrid molecules with two or more structural pharmacores having different biological functions and distinct activity have gained a significant role in cancer drug development to combat various types of malignancies. The present study describes an efficient, clean and strategic synthesis of 12 new substituted quinoline–indole–oxadiazole hybrids from substituted 2-(quinolin-8-yloxy)acetohydrazides and indole-3-carboxylic acids by employing T3P® as a green catalyst. Structures of the newly synthesized compounds were established by IR, ^{1}H NMR, ^{13}C NMR, DEPT C-NMR and MS spectroscopic evidence, as well as CHN analysis data. All indole–quinoline–oxadiazoles were tested for their in vitro cytotoxic potential in breast adenocarcinoma (MCF7) and normal kidney (vero) cell lines using MTT assay. 8-((5-(3-(1*H*-indol-3-yl)propyl)-1,3,4-oxadiazol-2-yl)methoxy)quinoline (**3d**) exhibited a low IC50 value and a high selectivity index to MCF7 cells and also displayed a mitotic block in flow cytometric cell cycle progression analysis. Microtubule disruption can induce G_2/M phase cell cycle arrest leading to abnormal mitotic spindle formation. Ligand **3d** demonstrated its capability of being a probable tubulin inhibitor when docked in the colchicine domain of tubulin.

Graphical Abstract New series of 8-((5-((1*H*-indol-3-yl)methyl)-1,3,4-oxadiazol-2-yl)methoxy)quinolines were synthesized using T3P® as a green catalyst and screened for their cytotoxic and antimitotic potential. The most active 8-((5-(3-(1*H*-indol-3-yl)propyl)-1,3,4-oxadiazol-2-yl)methoxy)quinoline **3d**, displayed good binding interactions with the colchicine binding cavity of microtubule.

✉ Dhanya Sunil
dhanyadss3@gmail.com

[1] Department of Chemistry, Manipal Institute of Technology, Manipal University, Manipal 576104, India

[2] Department of Atomic and Molecular Physics, Manipal Institute of Technology, Manipal University, Manipal, India

Published online: 14 January 2016

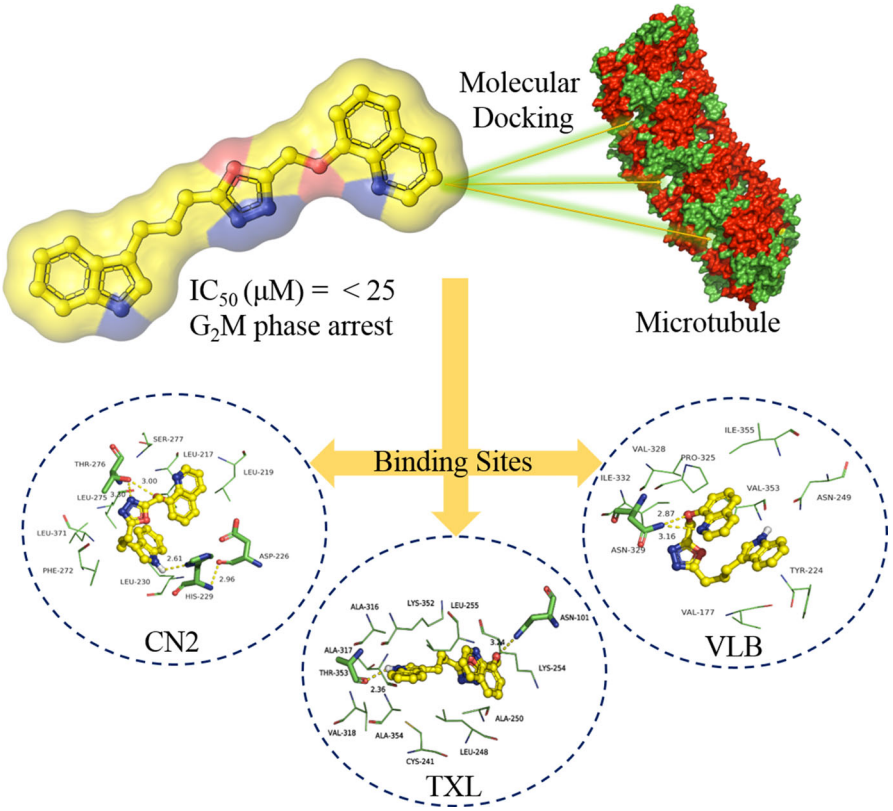

Keywords Indole–quinoline–oxadiazole · Cytotoxicity · Mitosis · Tubulin

Introduction

Cancer is becoming a worldwide pandemic and chemotherapy remains the most widely employed current treatment option. The failure of many successful contemporary chemotherapeutic drugs is mainly attributed to their side effects and the mechanism by which cancer cells develop resistance to these drugs, resulting in increased efflux of chemotherapeutic drugs from cancer cells. Hence, new advances in the development of anticancer drugs and more effective treatment approaches are of extreme relevance in drug discovery and chemotherapy. Based on considerable developments in cancer biology, major research in these areas is presently focused on developing drugs capable of reversing multidrug resistance with less toxic side effects that act via more cancer-specific mechanisms aimed at the corresponding molecular targets [1].

1,3,4-Oxadiazole, a heterocyclic nucleus, has been widely exploited for various spectra of therapeutic applications like HIV-integrase inhibitor raltagravir,

antibacterial furamizole, antihypertensive agents tiodazosin and nesapidil and anticancer agent zibotentan [2–6]. Past literature also discloses the extensive therapeutic potential and attractive anticancer activity of 1,3,4-oxadiazole incorporated with a highly biologically potent indole pharmacore [7–11]. The prominent role of the active quinoline nucleus has been well known in the search for molecules of pharmaceutical interest [12–18]. The present study aims at a propyl phosphonic acid cyclic anhydride (T3P®) mediated efficient cyclodehydration synthetic strategy of 1,3,4-oxadiazole template linking the two bioactive indole and quinoline moieties under mild reaction conditions with easy work-up procedures yielding pure products.

Microtubules, a major component of the eukaryotic cytoskeleton, play a crucial role during mitosis in proper spindle formation and are among the most effective and promising targets for anticancer therapy. Microtubule targeting drugs interact with tubulin primarily through three different binding sites: the taxane widely used in the treatment of lung, breast, ovarian and bladder cancers binds at the inner surface of the β subunit promoting tubulin stabilization; vinca alkaloids employed in the treatment of leukaemia, bladder and breast cancer bind with high affinity to one or few tubulin molecules at the tip of microtubules promoting depolymerization; and colchicine interacts with β-tubulin at its interface with α-tubulin, resulting in inhibition of tubulin polymerization [19, 20]. The limitations of current anti-tubulin drugs like drug resistance, toxicity and bioavailability warrants the identification of new potent tubulin inhibitors. The current work also focuses on the in vitro anticancer activity of the synthesized hybrid molecules and their in silico docking studies with tubulin as the target to explore their potential as microtubule inhibitors.

Experimental section

Chemistry

Chemicals and solvents for the present study were procured commercially from Sigma Aldrich, Merck and Himedia. Thin layer chromatography was performed using pre-coated aluminum sheets with Aluchrosep Silica Gel 60/UV254 and the spots were visualized in a UV chamber. Melting points of synthesized 1,3,4-oxadiazoles were checked by the open capillary method and are uncorrected. IR spectra in KBr pellets, NMR spectra with tetramethylsilane as internal standard and mass spectra were recorded in a Schimadzu FTIR 8400S spectrophotometer, Bruker 400 MHz instrument and Agilent 6510 series mass spectrometer, respectively. Elemental analysis of the compounds was carried out using a Flash thermo 1112 series CHN analyser.

General procedure for preparation of 8-((5-((1H-indol-3-yl)methyl)-1,3,4-oxadiazol-2-yl)methoxy)quinolines ***3(a–l)*** 2-(Quinolin-8-yloxy)acetohydrazides **1(a–c)** (1 mmol) and indole 3-carboxylic acids **2(a–d)** (1 mmol) was refluxed in nitrogen atmosphere with T3P® (2 mmol) and TEA (4 mmol) in ethyl acetate medium for 7 h at 80 °C. The reaction mixture was cooled, poured on to ice-cold sodium

bicarbonate solution and extracted with ethyl acetate. The organic solvent was evaporated and the crude product was re-crystallized from hexane.

*8-((5-(1H-indol-3-yl)-1,3,4-oxadiazol-2-yl)methoxy)quinoline (**3a**)* Dark brown solid (92.23 %); m.p. 178–180 °C; IR (KBr) [cm^{-1}]: 3207 (indole NH *str.*), 3062 (Ar. C–H *str.*), 2983 (methylene C–H *asym. str.*), 2858 (methylene C–H *sym. str.*), 1620 (C=N *str.*), 1573 (Ar. C=C *str.*), 1259 (C–O–C *str.*); ^{1}H NMR (400 MHz, DMSO-d_6) [ppm]: δ 4.83 (s, 2H, OCH_2), δ 6.95 (s, 1H, indole 2-H), δ 7.06 (d, 2H, quinoline 5-H and 7-H), δ 7.34–7.29 (m, 2H, quinoline 3-H and 6-H), δ 7.59–7.53 (m, 4H, indole), δ 8.34 (d, 1H, quinoline 4-H), δ 8.90 (d, 1H, quinoline 2-H), δ 9.90 (s, 1H, indole N–H); ^{13}C NMR (100 MHz, DMSO-d_6) δ = 174.97, 171.49, 149.75, 140.33, 136.79, 136.59, 129.65, 127.63, 127.29, 122.78, 122.47, 121.56, 121.29, 118.77, 118.71, 118.58, 114.49, 114.33, 112.30, 68.49; MS (*m*/*z*): 343 (M + 1); Anal. Calcd. for $C_{20}H_{14}N_4O_2$: C, 70.17; H, 4.12; N, 16.37; found: C, 70.37; H, 4.14; N, 16.39.

*8-((5-((1H-indol-3-yl)methyl)-1,3,4-oxadiazol-2-yl)methoxy)quinoline (**3b**)* Dark brown solid (87.78 %); m.p. 128–130 °C; IR (KBr) [cm^{-1}]: 3238 (indole NH *str.*), 3060 (Ar. C–H *str.*), 2983 (methylene C–H *asym. str.*), 2844 (methylene C–H *sym. str.*), 1618 (C=N *str.*), 1571 (Ar. C=C *str.*), 1259 (C–O–C *str.*); ^{1}H NMR (400 MHz, DMSO-d_6) [ppm]: δ 2.74 (s, 2H, CH_2), δ 4.85 (s, 2H, OCH_2), δ 6.93 (s, 1H, indole 2-H), δ 7.07 (d, 2H, quinoline 5-H and 7-H), δ 7.35–7.30 (m, 2H, quinoline 3-H and 6-H), δ 7.59–7.53 (m, 4H, indole), δ 8.37 (d, 1H, quinoline 4-H), δ 8.83 (d, 1H, quinoline 2-H), δ 9.89 (s, 1H, indole N–H); ^{13}C NMR (100 MHz, DMSO-d_6) δ = 174.95, 171.48, 149.75, 140.30, 136.77, 136.58, 129.63, 127.62, 127.28, 122.75, 122.45, 121.57, 121.28, 118.78, 118.73, 118.55, 114.48, 114.34, 112.33, 68.49, 31.88; MS (*m*/*z*): 357 (M + 1); Anal. Calcd. for $C_{20}H_{16}N_4O_2$: C, 70.77; H, 4.53; N, 15.72; found: C, 70.82; H, 4.54; N, 15.75.

*8-((5-(2-(1H-indol-3-yl)ethyl)-1,3,4-oxadiazol-2-yl)methoxy)quinoline (**3c**)* Light brown solid (90.59 %); m.p. 232–234 °C; IR (KBr) [cm^{-1}]: 3218 (indole NH *str.*), 3060 (Ar. C–H *str.*), 2948 (methylene C–H *asym. str.*), 2850 (methylene C–H *sym. str.*), 1618 (C=N *str.*), 1571 (Ar. C=C *str.*), 1259 (C–O–C *str.*); ^{1}H NMR (400 MHz, DMSO-d_6) [ppm]: δ 2.23 (t, 2H, CH_2), δ 2.72 (t, 2H, CH_2), δ 4.85 (s, 2H, OCH_2), δ 6.93 (s, 1H, indole 2-H), δ 7.11 (d, 2H, quinoline 5-H and 7-H), δ 7.32–7.27 (m, 2H, quinoline 3-H and 6-H), δ 7.59–7.52 (m, 4H, indole), δ 8.33 (d, 1H, quinoline 4-H), δ 8.87 (d, 1H, quinoline 2-H), δ 9.93 (s, 1H, indole N–H); ^{13}C NMR (100 MHz, DMSO-d_6) δ = 174.98, 171.48, 149.76, 140.32, 136.76, 136.53, 129.61, 127.65, 127.23, 122.77, 122.48, 121.55, 121.29, 118.76, 118.71, 118.57, 114.47, 114.33, 112.35, 68.41, 33.87, 33.42; MS (*m*/*z*): 371 (M + 1); Anal. Calcd. for $C_{22}H_{18}N_4O_2$: C, 71.34; H, 4.90; N, 15.13; found: C, 71.49; H, 4.92; N, 15.16.

*8-((5-(3-(1H-indol-3-yl)propyl)-1,3,4-oxadiazol-2-yl)methoxy)quinoline (**3d**)* Light brown solid (91.13 %); m.p. 242–244 °C; IR (KBr) [cm^{-1}]: 3332 (indole NH *str.*), 3049 (Ar. C–H *str.*), 2929 (methylene C–H *asym. str.*), 2835 (methylene C–H *sym. str.*), 1614 (C=N *str.*), 1564 (Ar. C=C *str.*), 1259 (C–O–C *str.*); ^{1}H NMR (400 MHz, DMSO-d_6) [ppm]: δ 1.88 (t, 2H, CH_2), δ 2.21 (m, 2H, CH_2), δ 2.70 (t,

2H, CH_2), δ 4.86 (s, 2H, OCH_2), δ 6.96 (s, 1H, indole 2-H), δ 7.08 (d, 2H, quinoline 5-H and 7-H), δ 7.33–7.28 (m, 2H, quinoline 3-H and 6-H), δ 7.58–7.52 (m, 4H, indole), δ 8.36 (d, 1H, quinoline 4-H), δ 8.88 (d, 1H, quinoline 2-H), δ 9.91 (s, 1H, indole N–H); ^{13}C NMR (100 MHz, DMSO-d_6) δ = 174.99, 171.49, 149.77, 140.30, 136.78, 136.51, 129.60, 127.62, 127.20, 122.79, 122.46, 121.53, 121.28, 118.79, 118.73, 118.56, 114.46, 114.37, 112.36, 68.40, 33.89, 33.44, 26.38; MS (*m*/*z*): 385 (M + 1); Anal. Calcd. for $C_{23}H_{20}N_4O_2$: C, 71.86; H, 5.24; N, 14.57; found: C, 72.05; H, 5.26; N, 14.60.

*8-((5-(1H-indol-3-yl)-1,3,4-oxadiazol-2-yl)methoxy)-2-methylquinoline (**3e**)* Cream solid (85.28 %); m.p. 128–130 °C; IR (KBr) [cm^{-1}]: 3211 (indole NH *str.*), 3062 (Ar. C–H *str.*), 2929 (methylene C–H *asym. str.*), 2862 (methylene C–H *sym. str.*), 1627 (C=N *str.*), 1569 (Ar. C=C *str.*), 1238 (C–O–C *str.*); ^{1}H NMR (400 MHz, DMSO-d_6) [ppm]: δ 2.48 (s, 3H, CH_3), δ 4.80 (s, 2H, OCH_2), δ 6.91 (s, 1H, indole 2-H), δ 7.05 (d, 2H, quinoline 5-H and 7-H), δ 7.36–7.30 (m, 1H, quinoline 6-H), δ 7.58–7.52 (m, 4H, indole), δ 8.35 (d, 2H, quinoline 3-H and 4-H), δ 9.92 (s, 1H, indole N–H); ^{13}C NMR (100 MHz, DMSO-d_6) δ = 174.96, 171.50, 150.75, 140.31, 136.78, 136.57, 129.64, 127.65, 127.27, 122.79, 122.47, 121.57, 121.28, 112.03 118.76, 118.73, 118.59, 114.48, 114.32, 68.47, 27.32; MS (*m*/*z*): 357 (M + 1); Anal. Calcd. for $C_{22}H_{16}N_4O_2$: C, 70.77; H, 4.53; N, 15.72; found: C, 71.02; H, 4.54; N, 15.76.

*8-((5-((1H-indol-3-yl)methyl)-1,3,4-oxadiazol-2-yl)methoxy)-2-methylquinoline (**3f**)* Light brown solid (93.21 %); m.p. 208–210 °C; IR (KBr) [cm^{-1}]: 3290 (indole NH *str.*), 3050 (Ar. C–H *str.*), 2921 (methylene C–H *sym. str.*), 2875 (methylene C–H *asym. str.*), 1666 (C=N *str.*), 1566 (Ar. C=C *str.*), 1234 (C–O–C *str.*); ^{1}H NMR (400 MHz, DMSO-d_6) [ppm]: δ 2.47 (s, 3H, CH_3), δ 2.73 (s, 2H, CH_2), δ 4.83 (s, 2H, OCH_2), δ 6.93 (s, 1H, indole 2-H), 7.06 (d, 2H, quinoline 5-H and 7-H), δ 7.35–7.29 (m, 1H, quinoline 6-H), δ 7.59–7.53 (m, 4H, indole), δ 8.37 (d, 2H, quinoline 3-H and 4-H), δ 9.94 (s, 1H, indole N–H); ^{13}C NMR (100 MHz, DMSO-d_6) δ = 174.95, 171.52, 150.74, 140.30, 136.76, 136.56, 129.63, 127.62, 127.26, 122.77, 122.46, 121.55, 121.28, 112.04, 118.75, 118.72, 118.58, 114.47, 114.30, 68.46, 31.87, 27.33; MS (*m*/*z*): 371 (M + 1); Anal. Calcd. for $C_{22}H_{18}N_4O_2$: C, 71.34; H, 4.90; N, 15.13; found: C, 71. 53; H, 4. 91; N, 15.16.

*8-((5-(2-(1H-indol-3-yl)ethyl)-1,3,4-oxadiazol-2-yl)methoxy)-2-methylquinoline (**3g**)* Dark brown solid (92.57 %); m.p. 230–232 °C; IR (KBr) [cm^{-1}]: 3232 (indole NH *str.*), 3055 (Ar. C–H *str.*), 2947 (methylene C–H *asym. str.*), 2830 (methylene C–H *sym. str.*), 1652 (C=N *str.*), 1566 (Ar. C=C *str.*), 1234 (C–O–C *str.*); ^{1}H NMR (400 MHz, DMSO-d_6) [ppm]: δ 2.22 (t, 2H, CH_2), δ 2.45 (s, 3H, CH_3), δ 2.70 (t, 2H, CH_2), δ 4.82 (s, 2H, OCH_2), δ 6.94 (s, 1H, indole 2-H), δ 7.08 (d, 2H, quinoline 5-H and 7-H), δ 7.33–7.27 (m, 1H, quinoline 6-H), δ 7.58–7.52 (m, 4H, indole), δ 8.38 (d, 2H, quinoline 3-H and 4-H), δ 9.95 (s, 1H, indole N–H); ^{13}C NMR (100 MHz, DMSO-d_6) δ = 174.93, 171.50, 150.73, 140.29, 136.75, 136.54, 129.62, 127.61, 127.25, 122.75, 122.44, 121.53, 121.26, 121.05, 118.74, 118.71, 118.55, 114.47, 114.28, 112.08, 68.45, 33.86, 33.40, 27.31; MS (*m*/*z*): 385 (M + 1); Anal.

Calcd. for $C_{23}H_{20}N_4O_2$: C, 71.86; H, 5.24; N, 14.57; found: C, 72.11; H, 5.25; N, 14.60.

8-((5-(3-(1H-indol-3-yl)propyl)-1,3,4-oxadiazol-2-yl)methoxy)-2-methylquinoline ***(3h)*** Dark brown solid (97.25 %); m.p. 162–164 °C; IR (KBr) [cm^{-1}]: 3265 (indole NH *str.*), 3056 (Ar. C–H *str.*), 2935 (methylene C–H *asym. str.*), 2890 (methylene C–H *sym. str.*), 1652 (C=N *str.*), 1566 (Ar. C=C *str.*), 1234 (C–O–C *str.*); ^{1}H NMR (400 MHz, DMSO-d_6) [ppm]: δ 1.87 (t, 2H, CH_2), δ 2.20 (m, 2H, CH_2), δ 2.42 (s, 3H, CH_3), δ 2.72 (t, 2H, CH_2), δ 4.80 (s, 2H, OCH_2), δ 6.92 (s, 1H, indole 2-H), δ 7.06 (d, 2H, quinoline 5-H and 7-H), δ 7.32–7.26 (m, 1H, quinoline 6-H), δ 7.56–7.50 (m, 4H, indole), δ 8.37 (d, 2H, quinoline 3-H and 4-H), δ 9.96 (s, 1H, indole N–H); ^{13}C NMR (100 MHz, DMSO-d_6) δ = 174.91, 171.49, 150.70, 140.25, 136.74, 136.51, 129.60, 127.63, 127.22, 122.71, 122.42, 121.50, 121.25, 118.70, 118.73, 118.54, 114.46, 114.27, 112.10, 68.43, 33.85, 33.41, 28.38 27.31; MS (*m/z*): 399 (M + 1); Anal. Calcd. for $C_{24}H_{22}N_4O_2$: C, 72.34; H, 5.57; N, 14.06; found: C, 72.44; H, 5.58; N, 14.09.

8-((5-(1H-indol-3-yl)-1,3,4-oxadiazol-2-yl)methoxy)-2,4-dichloroquinoline ***(3i)*** Brown solid (89.98 %); m.p. 254–256 °C; IR (KBr) [cm^{-1}]: 3261 (indole NH *str.*), 3085 (Ar. C–H *str.*), 2947 (methylene C–H *asym. str.*), 2858 (methylene C–H *sym. str.*), 1677 (C=N *str.*), 1566 (Ar. C=C *str.*), 1234 (C–O–C *str.*); ^{1}H NMR (400 MHz, DMSO-d_6) [ppm]: δ 4.96 (s, 2H, OCH_2), δ 7.01–6.97 (t, 1H, indole 5-H), δ 7.08–7.05 (t, 1H, indole 6-H), δ 7.18 (s, 1H, indole 2-H), δ 7.36 (d, 1H, indole 4-H), δ 7.58 (d, 1H, indole 7-H), δ 7.82–7.81 (m, 1H, quinoline 3-H), δ 8.05 (s, 1H, quinoline 6-H), δ 8.64 (d, 1H, quinoline 4-H), δ 8.97 (d, 1H, quinoline 2-H), δ 10.18 (s, 1H, indole N–H); ^{13}C NMR (100 MHz, DMSO-d_6) δ = 172.00, 170.59, 155.73, 149.68, 140.31, 136.72, 136.60, 128.19, 126.29, 123.83, 122.78, 121.40, 118.80, 118.65, 118.54, 114.47, 114.36, 112.37, 111.78, 72.73; MS (*m/z*): 412 (M + 1), 414 (M + 3), 416 (M + 5); Anal. Calcd. for $C_{20}H_{12}Cl_2N_4O_2$: C, 58.41; H, 2.94; N, 13.62; found: 58.61; H, 2.95; N, 13.66.

8-((5-((1H-indol-3-yl)methyl)-1,3,4-oxadiazol-2-yl)methoxy)-2,4-dichloroquinoline ***(3j)*** Brown solid (90.28 %); m.p. 258–260 °C; IR (KBr) [cm^{-1}]: 3250 (indole NH *str.*), 3091 (Ar. C–H *str.*), 2906 (methylene C–H *asym. str.*), 2840 (methylene C–H *sym. str.*), 1620 (C=N *str.*), 1564 (Ar. C=C *str.*), 1260 (C–O–C *str.*); ^{1}H NMR (400 MHz, DMSO-d_6) [ppm]: δ 2.56 (s, 2H, CH_2), δ 4.93 (s, 2H, OCH_2), δ 7.03–6.99 (t, 1H, indole 5-H), δ 7.09–7.06 (t, 1H, indole 6-H), δ 7.15 (s, 1H, indole 2-H), δ 7.35 (d, 1H, indole 4-H), δ 7.56 (d, 1H, indole 7-H), δ 7.80–7.79 (m, 1H, quinoline 3-H), δ 8.04 (s, 1H, quinoline 6-H), δ 8.63 (d, 1H, quinoline 4-H), δ 8.99 (d, 1H, quinoline 2-H), δ 10.14 (s, 1H, indole N–H); ^{13}C NMR (100 MHz, DMSO-d_6) δ = 172.01, 170.58, 155.75, 149.66, 140.32, 136.71, 136.61, 128.18, 126.28, 123.85, 122.77, 121.41, 118.82, 118.67, 118.53, 114.46, 114.35, 112.38, 111.79, 72.70, 31.20; MS (*m/z*): 426 (M + 1), 428 (M + 3), 430 (M + 5); Anal. Calcd. for $C_{21}H_{14}Cl_2N_4O_2$: C, 59.31; H, 3.32; N, 13.17; found: 59.53; H, 3.34; N, 13.20.

8-((5-(2-(1H-indol-3-yl)ethyl)-1,3,4-oxadiazol-2-yl)methoxy)-2,4-dichloroquinoline ***(3k)*** Brown solid (90.28 %); m.p. 240–242 °C; IR (KBr) [cm^{-1}]: 3205 (indole NH

str.), 3058 (Ar. C–H *str.*), 2933 (methylene C–H *asym. str.*), 2869 (methylene C–H *sym. str.*), 1685 (C=N *str.*), 1591 (Ar. C=C *str.*), 1230 (C–O–C *str.*); ^{1}H NMR (400 MHz, DMSO-d_6) [ppm]: δ 2.57 (t, 2H, CH_2), δ 2.96 (t, 2H, CH_2), δ 4.96 (s, 2H, OCH_2), δ 7.00–6.98 (t, 1H, indole 5-H), δ 7.08–7.05 (t, 1H, indole 6-H), δ 7.16 (s, 1H, indole 2-H), δ 7.33 (d, 1H, indole 4-H), δ 7.55 (d, 1H, indole 7-H), δ 7.79–7.78 (m, 1H, quinoline 3-H), δ 8.02 (s, 1H, quinoline 6-H), δ 8.61 (d, 1H, quinoline 4-H), δ 8.98 (d, 1H, quinoline 2-H), δ 10.15 (s, 1H, indole N–H); ^{13}C NMR (100 MHz, DMSO-d_6) δ = 171.99, 170.57, 155.71 149.67, 140.32, 136.71, 136.58, 128.17, 126.28, 123.84, 122.77, 121.39, 118.79, 118.67, 118.56, 114.46, 114.37, 112.39, 111.79, 72.74, 34.46, 33.49; MS (*m/z*): 440 (M + 1), 442 (M + 3), 444 (M + 5); Anal. Calcd. for $C_{22}H_{16}Cl_2N_4O_2$: C, 60.15; H, 3.67; N, 12.75; found: 60.34; H, 3.69; N, 12.78.

8-((5-(3-(1H-indol-3-yl)propyl)-1,3,4-oxadiazol-2-yl)methoxy)-2,4-dichloroquinoline ***(3l)*** Dark red solid (94.07 %); m.p. 184–186 °C; IR (KBr) [cm^{-1}]: 3267 (indole NH *str.*), 3058 (Ar. C–H *str.*), 2933 (methylene C–H *asym. str.*), 2839 (methylene C–H *sym. str.*), 1608 (C=N *str.*), 1577 (Ar. C=C *str.*), 1240 (C–O–C *str.*); ^{1}H NMR (400 MHz, DMSO-d_6) [ppm]: δ 1.86 (t, 2H, CH_2), δ 2.56–2.54 (m, 2H, CH_2), δ 2.95 (t, 2H, CH_2), δ 4.97 (s, 2H, OCH_2), δ 7.01–6.97 (t, 1H, indole 5-H), δ 7.06–7.03 (t, 1H, indole 6-H), δ 7.18 (s, 1H, indole 2-H), δ 7.32 (d, 1H, indole 4-H), δ 7.56 (d, 1H, indole 7-H), δ 7.77–7.75 (m, 1H, quinoline 3-H), δ 8.06 (s, 1H, quinoline 6-H), δ 8.63 (d, 1H, quinoline 4-H), δ 8.96 (d, 1H, quinoline 2-H), δ 10.11 (s, 1H, indole N–H); ^{13}C NMR (100 MHz, DMSO-d_6) δ = 172.07, 170.60, 155.73, 149.68, 140.33, 136.75, 136.62, 128.19, 126.27, 123.86, 122.78, 121.42, 118.83, 118.69, 118.51, 114.48, 114.33, 112.39, 111.77, 72.68, 34.45, 33.50, 27.39; MS (*m/z*): 454 (M + 1), 456 (M + 3), 458 (M + 5); Anal. Calcd. for $C_{23}H_{18}Cl_2N_4O_2$: C, 60.94; H, 4.00; N, 12.36; found: 61.14; H, 4.02; N, 12.39.

Biological studies

Anticancer studies

MCF-7 and non-cancerous kidney vero cell lines, procured from the National Centre for Cancer Studies, Pune, India, were cultured at 37 °C in 5 % CO_2 atmosphere in Dulbecco's modified Eagles medium containing 10 % fetal bovine serum.

MTT assay

MTT is a standard in vitro colorimetric assay used to monitor the extent of cell proliferation and viability as well as cytotoxicity. The MCF7 and normal vero cells were trypsinized and counted using standard procedures. Cells were seeded at a density of 5 × 10^3 cells in 96-well plates and were incubated at 37 °C for 24 h in CO_2 atmosphere. Subsequently, cells were treated with different concentrations of test compounds (50–400 μM) in triplicates and incubated for 48 h at 37 °C. Vehicles and their dilutions used to dissolve the test compounds were used as controls. After 24 h, 30 μL of MTT reagent (4 mg/mL) was added to each well and

further incubated for an additional 4 h at 37 °C. Plates were centrifuged, media was aspirated, 100 µL of DMSO was used to dissolve the formazan crystals and finally the optical density was noted at 540 nm in an ELISA plate reader (ELx800; BioTek, VT, USA) [21, 22].

Flow cytometry

Flow cytometric cell sorter analysis was performed to study the effect of test compounds on cell cycle progression. Around 2×10^6 cells/mL were cultured and incubated for 48 h with 0.5 µM vincristine and 5 µM test compound. Later, the cells were washed with ice-cold PBS and fixed with 2 mL of 70 % ice-cold alcohol for 30 min at 4 °C. Then, the cells were centrifuged, and the alcohol was discarded and washed with 2 mL phosphate buffer saline (PBS). About 100 mg/L of RNase was added to the pellets and incubated for 1 h at room temperature. Then, 1 mL of PBS and 5 g/L of propidium iodide was added and incubated for 30 min in the dark. Finally, the cells were acquired using a BD Accuri™ C6 flow cytometer and cell cycle distribution was examined [21].

In-silico molecular modelling and docking studies

Microtubules are heterodimers consisting of α- and β-tubulin with 453 and 455 amino acids, respectively, and are critical for cell growth and proliferation. They undergo conformational changes and switch from straight to curved conformation or vice versa based on the inhibitors. Tubulin inhibitors are classified based on their microtubule stabilizing and destabilizing mechanism. Tubulin has three major binding sites, one each for taxol and vinca-alkaloids which cause microtubule polymerization and one for colchicine that acts via a microtubule depolymerisation mechanism. Hence, microtubule dynamics is an important target for anticancer drug discovery and docking studies has been carried out with **3d** in all the three major inhibitor sites. The structure of the ligand molecules—colchicine (CN2), docetaxel (TXL), vinblastine (VLB) and **3d** in MDL format—were drawn using MarvinSketch 14.11.17.0 (http://www.chemaxon.com). The MOL2 format of these structures was generated using Open Babel software [23]. As of now, α and β tubulin protein date bank (PDB) has eight tubulin structures complexed with CN2 (PDB IDs: 1SA0, 1Z2B, 3DU7, and 4O2B), TXL (PDB ids: 1IA0, and 1TUB) and VLB (PDB ids: 1Z2B, and 4EB6). High-resolution tubulin crystal structures complexed with CN2 (PDB ID: 1SA0), TXL (PDB ID: 1TUB) and VLB (PDB ID: 1Z2B) were selected from α and β tubulin PDB for further studies. Input files necessary for docking studies were prepared by removing the bound ligands, ions and water, and later polar hydrogen atoms were added to the protein molecule using AutoDockTools (v.1.5.6) [24]. The grid maps were created for both receptor and ligands based on the corresponding ligand binding sites. The docking studies were performed using AutoDock Vina (v.1.1.2) [25] and the docking parameters were kept as default values. Molecular interactions were calculated using CONTACT program accessible in CCP4 suite [26] and surface area specifications were calculated by the PDBePISA server (http://www.ebi.ac.uk/msd-srv/prot_int/cgi-bin/piserver). The

structural models were generated by Pymol (www.pymol.org, PyMol-Version 1.6. Schrödinger, LLC.).

Results and discussion

Chemistry

Indole-3-carboxylic acids **1(a–c)** were appropriately selected to fix four different alkyl chain spacers at α and β tubulin C-5 position of α and β tubulin oxadiazole ring for the present study. Substituted 2-(quinolin-8-yloxy)acetohydrazides **2(a–d)** were prepared from substituted quinolin-8-ols via two-step reaction methods as provided by α and β tubulin literature [27]. The cyclization reaction of equimolar quantities of indole-3-carboxylic acids **2(a–d)** and 2-(quinolin-8-yloxy)acetohydrazides **1(a–c)** were carried out in nitrogen atmosphere using T3P® to synthesize the respective indole–quinoline–oxadiazoles **3(a–l)** [28]. The advantages of T3P®, like less tedious work-up processes and pure products with better yield, wwereas exploited in the current cyclization reaction. The reaction conditions were optimized by changing the molar ratios of T3P® and TEA (triethyl amine) under various reaction temperatures and reaction times. Equimolar amounts of reactants **1(a–c)** and **2(a–d)** with 2 equivalent of T3P® and 4 equivalent of TEA on refluxing in ethyl acetate medium at 80 °C for 7 h indicated pure product formation. The synthetic pathway of 8-((5-((1*H*-indol-3-yl)methyl)-1,3,4-oxadiazol-2-yl)methoxy)quinoline derivatives **3(a–l)** is depicted in Scheme 1.

The T3P®-mediated dehydration mechanism of acid and hydrazide involves the well-established conversion of the oxygen of indole-3-carboxylic acid into an ionic leaving group that will lead to the formation of 1,2-diacyl hydrazines **I** (Fig. 1). The phosphorous atom of T3P® will then attack the oxygen of the carbonyl group of 1,2-diacyl hydrazine **I** to produce an intermediate **II** that would further cyclize to intermediate **III**, followed by nitrogen-aided removal of the anion to give the final oxadiazole derivative **IV**. The ionic byproduct can be easily extracted by aqueous work-up with minor product loss. The proposed cyclodehydration mechanism supported by T3P® is outlined in Fig. 1.

The carbonyl absorption peaks of the two reactants, 2-(quinolin-8-yloxy)acetohydrazides and indole-3-carboxylic acids, were observed at 1670–1680 and 1715–1725 cm^{-1} in their respective IR spectra. The absence of these carbonyl absorptions in the IR spectra of oxadiazole confirms the formation of the cyclized product. The ^{1}H NMR of the reactants showed signals at 2 ppm that corresponds to NH_2 protons and 11 ppm for the acid proton. These characteristic peaks were also not observed in the ^{1}HNMR spectra of oxadiazoles which further substantiates the complete cyclization of the reactants. The OCH_2 protons of oxadiazoles were found to resonate in the deshielded region at 4.80–4.97 ppm, while the methylene protons were observed upfield in the range of 1.8–2.7 ppm, which was further confirmed by the DEPT C NMR-spectra. The mass spectra of oxadiazoles displayed the molecular ion peaks as per their respective molecular masses.

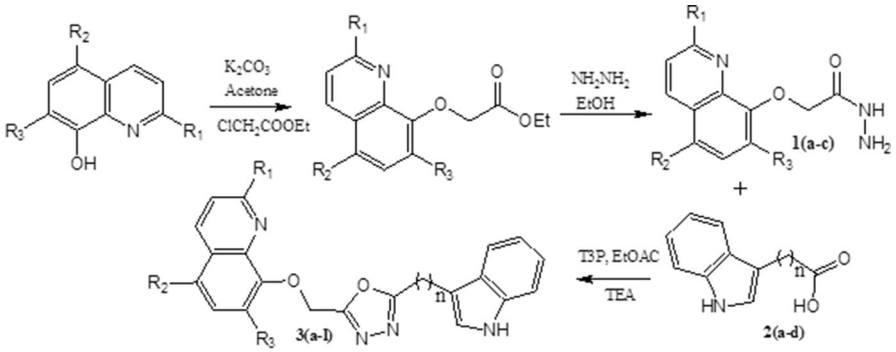

Comp. No.	n	R_1	R_2	R_3	Comp. No.	n	R_1	R_2	R_3
1a	-	H	H	H	**3d**	3	H	H	H
1b	-	CH_3	H	H	**3e**	0	CH_3	H	H
1c	-	H	Cl	Cl	**3f**	1	CH_3	H	H
2a	0	-	-	-	**3g**	2	CH_3	H	H
2b	1	-	-	-	**3h**	3	CH_3	H	H
2c	2	-	-	-	**3i**	0	H	Cl	Cl
2d	3	-	-	-	**3j**	1	H	Cl	Cl
3a	0	H	H	H	**3k**	2	H	Cl	Cl
3b	1	H	H	H	**3l**	3	H	Cl	Cl
3c	2	H	H	H					

Scheme 1 Synthetic pathway for 8-((5-((1H-indol-3-yl)methyl)-1,3,4-oxadiazol-2-yl) methoxy)quinolines **3(a–i)**

Biological activity

All the synthesized oxadiazoles **(3a–l)** were subjected to MTT assay in order to analyze their in vitro cytotoxicity profile and the results are represented in Table 1. The assay was performed in triplicate and the results were statistically analyzed using Graph Pad Prism, 5. Compound **3d** was found to significantly reduce the viability of MCF7 cells with an IC_{50} value of 8.62 μM. It also displayed higher selectivity (fourfold) to breast adenocarcinoma cells than to vero cells, whereas the selectivity index of vincristine was three. The active compound **3d** is derived from indole-3-butyric acid and 2-(quinolin-8-yloxy)acetohydrazide.

Apoptosis induced by tubulin-interfering agents is widely testified to follow G2/M cell cycle arrest. To study the effect of compound **3d** on different phases of the MCF7 cell cycle, flow cytometric studies were carried out. A normal cell cycle pattern was observed in the histogram of DMSO-treated control cells is presented in Fig. 2. The standard antimitotic drug vincristine (0.5 μM), exhibited G_2/M phase cell cycle arrest in breast adenocarcinoma cells at the end of 48 h, as shown in Fig. 2. A cell cycle arrest in the mitotic phase was seen in the histogram of MCF7 cells when subjected to a 48-h treatment with oxadiazole **3d**. A lesser number of cells were observed in the S phase (7.2 %) when incubated with **3d** compared with

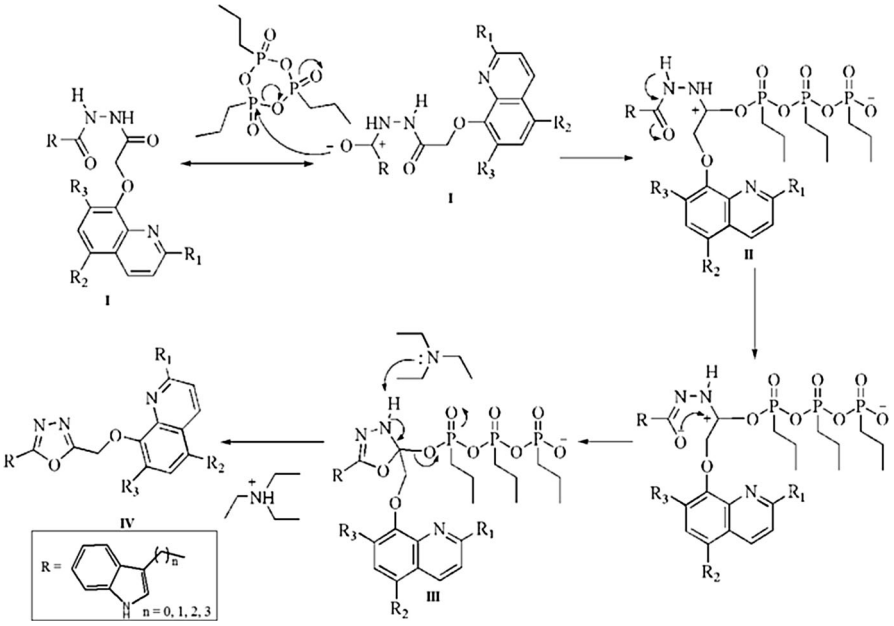

Fig. 1 Proposed mechanism for the formation of 1,3,4-oxadiazole mediated by T3P® and TEA

Table 1 In vitro cell growth inhibition by indole–quinoline–oxadiazole **3(a–l)** using MTT assay

Comp. no.	IC_{50} (μM) MCF-7	IC_{50} (μM) VERO
Vincristine	0.3 ± 0.02	0.9 ± 0.04
3a	205.5 ± 5.89	>200
3b	>200	>200
3c	>200	>200
3d	**8.62 ± 1.23**	**38.09 ± 1.87**
3e	>200	>200
3f	>200	>200
3g	>200	>200
3h	136.6 ± 3.57	>200
3i	>200	>200
3j	>200	>200
3k	>200	>200
3l	>200	>200

Bold distinguishes the most active molecule

control, with 11.8 % of MCF-7 cells permitting the cells to move to mitotic phase. Moreover, a rise in the number of mitotic cells from 19.5 % (as seen in the control) to 23.7 % in the **3d**-treated cells was visible in the cell cycle histogram, which is indicative of mitotic cell cycle arrest.

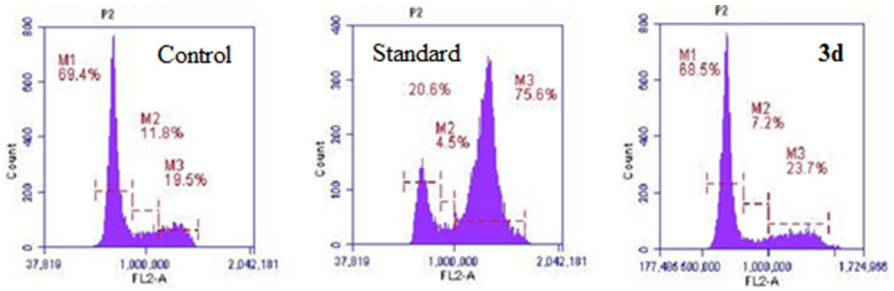

Fig. 2 Detection of cell cycle arrest using flow cytometry. A reduction in the percentage of cells in the S phase allowing cells to move into the mitotic phase and accumulation of cells in mitotic phase is seen in **3d**-treated cells when compared to control

Molecular modeling studies

The interaction of tubulin with a large number of drugs that inhibit or promote microtubule assembly has led to the identification of three drug binding sites, namely colchicine, taxol and vinca sites on the protein. In order to investigate the extent of interactions involved between the most active compound **3d** with the three known binding sites of microtubules, molecular docking studies were carried out. Initial docking was performed with the control molecules—colchicine, pacilitaxel, and vinblastine—to check the accuracy of molecular docking studies. Later, **3d** was docked into these binding sites with three separate seeds. Autodock Vina yielded 20 different conformations for each binding site. Selection of the final models was done based on the binding affinity values. The respective binding energies and computational molecular interaction details for each of the ligands are presented in Table 2. The binding affinities for all the controls were on par with the reported values. The superimposed models of **3d** and controls in their respective binding pockets are shown in Fig. 3. The binding models of **3d** to three tubulin binding sites are presented in Fig. 4. Oxadiazole **3d** was found to make hydrogen bonds with Asn101, Ala317 and Lys 352 amino acids when docked at the colchicine site. Interestingly, **3d** also covered similar orientation of colchicine (Fig. 3a) and was found to make hydrophobic contacts with seven amino acids (Table 2) identical to that observed with colchicine. This orientation played a key role in allowing the two nitrogen atoms of the oxadiazole ring of **3d** to make hydrogen bonds with the hydrogen attached to the hydroxyl groups of Lys353 (3.09 Å), Ala317 (2.36 Å) and amine group of Asn101 (3.24 Å) of the tubulin amino acids. The oxygen atom present between quinoline and oxadiazole moieties were involved in the interaction with tubulin amino acids apart from the nitrogen atoms in the rings. Surprisingly, the indole moiety of **3d** did not show any appreciable interaction with the tubulin amino acids. In the taxol binding site, **3d** was found to interact through two hydrogen bonds (His229 and Thr226) and eight hydrophobic contacts within the 4.0 Å cut-off from tubulin amino acids. In the crystal structure with tubulin, TXL also displayed similar hydrogen bonds with His229. Similar results were obtained when **3d** was docked at the VLB site. The hydrogen bond details and hydrophobic

Table 2 Docking results of ligand **3d** at colchicine, paclitaxel and vinblastine binding site of microtubule

	At colchicine binding site		At paclitaxel biding site		At vinblastine biding site	
	CN2[a]	**3d**	TXL[a]	**3d**	VLB[a]	**3d**
Molecular formula	$C_{22}H_{25}NO_6S$	$C_{23}H_{20}N_4O_2$	$C_{43}H_{53}NO_{14}$	$C_{23}H_{20}N_4O_2$	$C_{46}H_{58}N_4O_9$	$C_{23}H_{20}N_4O_2$
Molecular weight (g/mol)	431.50	384.439	807.88	384.439	810.97	384.439
Over all surface area (Å^2)	630	227	865	227	927	227
Binding affinity (kcal/mol)	−7.4	−9.3	−8.6	−8.7	−9.6	−7.2
Tubulin amino acids	Ser178	**Asn101**	Val23	Leu217	Lys176	*Val177*
	Val181	*Cys241*	*Asp226*	Leu219	*Val177*	*Tyr224*
	Cys241	*Leu248*	***His229***	*Asp226*	Tyr210	Asn249
	Leu242	*Ala250*	Ser236	***His229***	Phe214	*Pro325*
	Leu248	*Lys254*	*Phe272*	Leu230	Thr221	*Val328*
	Ala250	*Leu255*	*Leu275*	*Phe272*	Pro222	***Asn329***
	Lys254	*Ala316*	*Thr276*	*Leu275*	Thr223	Ile332
	Leu255	**Ala317**	Pro360	***Thr276***	*Tyr224*	***Val353***
	Asn258	Val318	Arg369	Ser277	Leu227	*Ile355*
	Met259	***Lys352***	Gly370	*Leu371*	*Pro325*	
	Ala316	Thr353	*Leu371*		*Val328*	
	Lys352	Ala354			*Val353*	
	Ile378				*Ile355*	
					Asn329	
Maximum interface area (Å^2)	407.2	124.7	557.7	139.8	335.8	129.3

Tubulin amino acids involved in possible hydrogen bonds are shown in bold

[a] Controls

contacts compared to VLB are summarized in Table 2. In general, the docking scores, molecular interactions and interaction surface obtained for **3d** well fitted with the colchicine site. The binding affinity and molecular interactions suggest better compatibility for **3d** with the colchicine site, in comparison with the TXL and VLB sites.

The introduction of methylene linkers between C-3 of the indole ring and C-5 of the oxadiazole moiety was reported to show promising activity [7, 21]. This study aims to incorporate diversity in methylene linker substitution at C-5 positions of the oxadiazole ring connected to C-3 of the highly bioactive indole group. The effect of

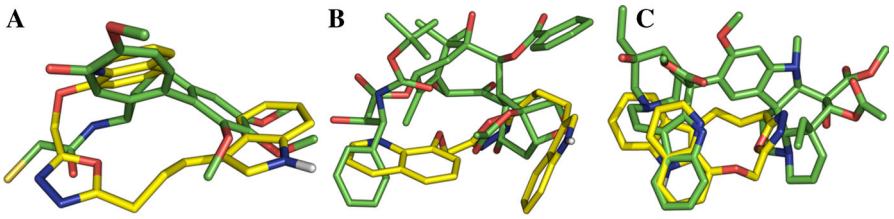

Fig. 3 Superimposed models of tubulin bound ligand **3d** on **a** colchicine, **b** pacilitaxel, and **c** vinblastine in their corresponding binding sites extracted from the crystal structures. Oxadiazole **3d:** carbon (*yellow*), oxygen (*red*), nitrogen (*dark blue*); CN2, TXL, VLB: carbon (*green*), nitrogen (*blue*) and oxygen (*red*). (Color figure online)

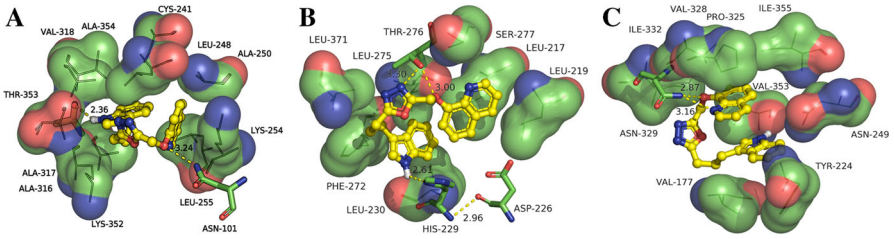

Fig. 4 Computational docking models: **3d** docked at **a** colchicine, **b** pacilitaxel, and **c** vinblastine sites of tubulin

the electron-donating methyl group and the electro-withdrawing chlorine atom attached to the quinoline moiety on the cytotoxic and antimitotic profile of indole–quinoline–1,3,4-oxadiazole derivatives was explored. The SAR study reveals that a longer three-methylene side chain linker ($n = 3$) at C-5 position of oxadiazole without any electron-donating or -withdrawing substituents on the quinoline ring has a relatively enhanced activity. The molecular docking results show that the nitrogens of the oxadiazole and quinoline rings are essential as recognition features with the key amino acid residues at the enzyme binding site for tubulin inhibition. A flexible oxo-methylene linker is essential to permit hydrophobic recognition of phenyl rings with the hydrophobic area of amino acids at the enzyme pocket [29]. The introduction of a methyl group at the C-2 position and two chloro substituents at the C-5 and C-7 positions of the quinoline ring did not increase the anticancer activity of the oxadiazole derivatives.

Conclusions

The present study discusses a convenient, efficient and green synthetic route to synthesize 12 new 8-((5-((1*H*-indol-3-yl)methyl)-1,3,4-oxadiazol-2-yl)methoxy)quinolines from substituted 2-(quinolin-8-yloxy) acetohydrazides and indole-3-carboxylic acids with T3P® as catalytic dehydrocyclization agent. Oxadiazole **3d** inhibited breast adenocarcinoma cell proliferation with a low IC_{50} value, high selectivity index and G2/

M cell cycle arrest advocating its potential to act as a lead anticancer and antimitotic molecule. Good binding interactions of oxadiazole **3d** with the colchicine binding cavity of microtubules correlates well with the antiproliferative activity and holds great promise as a potential tubulin inhibitor causing mitotic cell cycle arrest leading to apoptosis. Although colchicine is used in the treatment of gouty arthritis and familial Mediterranean fever, neither colchicine nor any related compounds bind to colchicine binding sites due to their toxicity. Based on these facts, **3d** and its derivatives may serve as a potent alternative.

Acknowledgment The authors are grateful to the Department of Science and Technology, Science and Engineering Research Board, India, for supporting the computational facilities through Grant SB/FT/LS-273/2012.

References

1. J.P. Gillet, M.M. Gottesman, Methods. Mol. Biol. **596**, 47 (2010). doi:10.1007/978-1-60761-416-6_4
2. R. Somani, A. Agrawal, P. Kalantri, P. Gavarkar, E.D. Clercq, Int. J. Drug Des. Discov. **2**, 353 (2011)
3. R.A. Rane, P. Bangalore, S.D. Borhade, P.K. Khandare, Eur. J. Med. Chem. **70**, 49 (2013). doi:10.1016/j.ejmech.2013.09.039
4. K. Zhang, P. Wang, L. Xuan, X. Fu, F. Jing, S. Li, Y. Liu, B. Chen, Bioorg. Med. Chem. Lett. **24**, 5154 (2014). doi:10.1016/j.bmcl.2014.09.086
5. A. Ramazani, M. Khoobi, A. Torkaman, F.Z. Nasrabadi, H. Forootanfar, M. Shakibaie, M. Jafari, A. Ameri, S. Emami, M.A. Faramarzi, A. Foroumadi, A. Shafiee, Eur. J. Med. Chem. **78**, 151 (2014). doi:10.1016/j.ejmech.2014.03.049
6. P. Puthiyapurayil, P. Boja, C. Chandrashekhar, B.S. Kumar, Eur. J. Med. Chem. **53**, 203 (2012). doi:10.1016/j.ejmech.2012.03.056
7. Y. Zhou, B. Wang, F. Di, L. Xiong, N. Yang, Y. Li, Y. Li, Z. Li, Bioorg. Med. Chem. Lett. **24**, 2295 (2014). doi:10.1016/j.bmcl.2014.03.077
8. N.I. Ziedan, F. Stefanelli, S. Fogli, A.D. Westwell, Eur. J. Med. Chem. **45**, 4523 (2010). doi:10.1016/j.ejmech.2010.07.012
9. D. Yang, P. Wang, J. Liu, H. Xing, Y. Liu, W. Xie, G. Zhao, Bioorg. Med. Chem. **22**, 366 (2014). doi:10.1016/j.bmc.2013.11.022
10. S. Rapolu, M. Alla, V.R. Bommena, R. Murthy, N. Jain, V.R. Bommareddy, M.R. Bommineni, Eur. J. Med. Chem. **66**, 91 (2013). doi:10.1016/j.ejmech.2013.05.024
11. D. Kumar, S. Sundaree, E. Johnson, K. Shah, ChemInform **40**, 4492 (2009). doi:10.1016/j.bmcl.2009.03.172
12. P. Srihari, B. Padmabhavani, S. Ramesh, Y.B. Kumar, A. Singh, R. Ummanni, Bioorg. Med. Chem. Lett. **25**, 2360 (2015). doi:10.1016/j.bmcl.2015.04.018
13. S.A. El-Feky, Z.K. Abd El-Samii, N.A. Osman, J. Lashine, M.A. Kamel, H.K.H. Thabet, Bioorg. Chem. **58**, 104 (2015). doi:10.1016/j.bioorg.2014.12.003
14. C.H. Tseng, C.C. Tzeng, C.Y. Hsu, C.M. Cheng, C.N. Yang, Y.L. Chen, Eur. J. Med. Chem. **97**, 306 (2015). doi:10.1016/j.ejmech.2015.04.054
15. M. Jelen, K. Pluta, K. Suwinska, B. Morak-Młodawska, M. Latocha, A. Shkurenko, J. Mol. Struct. **1099**, 10 (2015). doi:10.1016/j.molstruc.2015.06.046
16. K.S.S. Praveena, E.V.V. Shivaji, N.Y.S. Murthy, S. Akkenapally, C.G. Kumar, R. Kapavarapu, S. Pal, Bioorg. Med. Chem. Lett. **25**, 1057 (2015). doi:10.1016/j.bmcl.2015.01.012
17. M.J. Lai, J.Y. Chang, H.Y. Lee, C.C. Kuo, M.H. Lin, H.P. Hsieh, C.Y. Chang, J.S. Wu, S.Y. Wu, K.S. Shey, J.P. Liou, Eur. J. Med. Chem. **46**, 3623 (2011). doi:10.1016/j.ejmech.2011.04.065
18. I. Hatti, R. Sreenivasulu, S. Jadav, M. Ahsan, R. Raju, Monatsh. Chem. (2015). doi:10.1007/s00706-015-1448-1
19. R. Kaur, G. Kaur, R.K. Gill, R. Soni, J. Bariwal, Eur. J. Med. Chem. **87**, 89 (2014). doi:10.1016/j.ejmech.2014.09.051
20. Y. Lu, J. Chen, M. Xiao, W. Li, D.D. Miller, Pharm. Res. **29**, 2943 (2012). doi:10.1007/s11095-012-0828-z

21. P. Pozarowski, Z. Darzynkiewicz, Methods Mol. Biol. **281**, 301 (2004). doi:10.1385/1-59259-811-0:301
22. T. Mosmann, J. Immunol. Methods **16**, 55 (1983). doi:10.1016/0022-1759(83)90303-4
23. A.A. Waghmare, R.M. Hindupur, H.N. Pati, Rev. J. Chem. **4**, 53 (2014). doi:10.1134/S2079978014020034
24. N.M. O'Boyle, M. Banck, C.A. James, C. Morley, T. Vandermeersch, G.R. Hutchison, J. Cheminf. (2011). doi:10.1186/1758-2946-3-33
25. G.M. Morris, R. Huey, W. Lindstrom, M.F. Sanner, R.K. Belew, D.S. Goodsell, A.J. Olson, J. Comput. Chem. **30**, 2785 (2009). doi:10.1002/jcc.21256
26. O. Trott, A.J. Olson, J. Comput. Chem. **31**, 455 (2010). doi:10.1002/jcc.21334
27. M.V. Berridge, P.M. Herst, A.S. Tan, Biotechnol. Annu. Rev. **11**, 127 (2005). doi:10.1016/S1387-2656(05)11004-7
28. J.K. Augustine, V. Vairaperumal, S. Narasimhan, P. Alagarsamy, A. Radhakrishnan, Tetrahedron **65**, 9989 (2009). doi:10.1016/j.tet.2009.09.114
29. R.A. Laskowski, M.B. Swindells, J. Chem. Inf. Model. **51**, 2778 (2011). doi:10.1021/ci200227u